The Astrophysical Journal Letters, 863:L3 (7pp), 2018 August 10 https://doi.org/10.3847/2041-8213/aad59b
© 2018. The American Astronomical Society. All rights reserved.

Spectroscopic Investigation of a Reionized Galaxy Overdensity at $z = 7$

M. Castellano[1], L. Pentericci[1], E. Vanzella[2], F. Marchi[1], A. Fontana[1], P. Dayal[3], A. Ferrara[4], A. Hutter[5], S. Carniani[6,7], S. Cristiani[8,9], M. Dickinson[10], S. Gallerani[4], E. Giallongo[1], M. Giavalisco[11], A. Grazian[1], R. Maiolino[6,7], E. Merlin[1], D. Paris[1], S. Pilo[1], and P. Santini[1]

[1] INAF—Osservatorio Astronomico di Roma, Via Frascati 33, I-00040 Monte Porzio Catone (RM), Italy; marco.castellano@inaf.it
[2] INAF—Osservatorio Astronomico di Bologna, Via Ranzani 1, I-40127, Bologna, Italy
[3] Kapteyn Astronomical Institute, University of Groningen, P.O. Box 800, 9700, AV Groningen, The Netherlands
[4] Scuola Normale Superiore, Piazza dei Cavalieri 7, I-56126 Pisa, Italy
[5] Swinburne University of Technology, Hawthorn, VIC 3122, Australia
[6] Cavendish Laboratory, University of Cambridge, 19 J.J. Thomson Avenue, Cambridge CB3 0HE, UK
[7] Kavli Institute for Cosmology, University of Cambridge, Madingley Road, Cambridge CB3 0HA, UK
[8] INAF—Osservatorio Astronomico di Trieste, Via G.B. Tiepolo 11, I-34143 Trieste, Italy
[9] INFN—National Institute for Nuclear Physics, via Valerio 2, I-34127, Trieste, Italy
[10] National Optical Astronomy Observatories, Tucson, AZ 85719, USA
[11] Astronomy Department, University of Massachusetts, Amherst, MA 01003, USA
Received 2018 June 19; revised 2018 July 13; accepted 2018 July 23; published 2018 August 3

Abstract

We present deep spectroscopic follow-up observations of the Bremer Deep Field (BDF), where the two $z \sim 7$ bright Lyα emitters (LAE) BDF521 and BDF3299 were previously discovered by Vanzella et al. and where a factor of ∼3–4 overdensity of faint LBGs has been found by Castellano et al. We confirm a new bright Lyα emitter, BDF2195, at the same redshift of BDF521, $z = 7.008$ and at only ∼90 kpc physical distance from it, confirming that the BDF area is likely an overdense, reionized region. A quantitative assessment of the Lyα fraction shows that the number of detected bright emitters is much higher than the average found at $z \sim 7$, suggesting a high Lyα transmission through the intergalactic medium. However, the line visibility from fainter galaxies is at odds with this finding, as no Lyα emission is found in any of the observed candidates with $M_{\rm UV} > -20.25$. This discrepancy can be understood either if some mechanism prevents Lyα emission from fainter galaxies within the ionized bubbles from reaching the observer, or if faint galaxies are located outside the reionized area and bright LAEs are solely responsible for the creation of their own H II regions. A thorough assessment of the nature of the BDF region and of its sources of re-ionizing radiation will be made possible by *James Webb Space Telescope* spectroscopic capabilities.

Key words: dark ages, reionization, first stars – galaxies: evolution – galaxies: high-redshift

1. Introduction

The redshift evolution of the fraction of Lyman-break galaxies (LBGs) showing Lyα emission (e.g., Stark et al. 2010) allows us to put constraints on the Lyα transmission by the intergalactic medium (IGM). A substantial decrease of the Lyα fraction between $z \sim 6$ and $z \sim 7$ has been established by many independent analyses and interpreted as an indication of a neutral hydrogen fraction $\chi_{\rm H\,I} \sim 40\%$–$50\%$ at $z \sim 7$ (e.g., Fontana et al. 2010; Pentericci et al. 2011, 2014; Vanzella et al. 2011; Caruana et al. 2012; Schenker et al. 2012). The analysis of independent lines of sight presented in Pentericci et al. (2014; hereafter P14) has also shown that the decrease of the Lyα fraction suggests a patchy reionization process.

Among the eight pointings analyzed by P14, the Bremer Deep Field (BDF; Lehnert & Bremer 2003) stands out as a peculiar area in the $z \sim 7$ universe. In fact, a single FORS2 slit mask observation of this field yielded the detection of two bright ($L \sim L^*$) Lyα-emitting (LAE) galaxies, namely BDF3299 and BDF521, at $z = 7.109$ and $z = 7.008$, respectively (Vanzella et al. 2011, hereafter V11). These two objects, originally selected from our sample of Very Large Telescope (VLT)/Hawki-I z-dropout LBGs (Castellano et al. 2010, hereafter C10b), show Lyα equivalent widths >50 Å and are separated by a projected distance of only 1.9 Mpc, while the distance computed from Lyα redshifts is 4.4 Mpc (see V11). The detection of bright Lyα emission from BDF3299 and BDF521 can be explained by these sources being embedded in an H II region that allows Lyα photons to redshift away from resonance before they reach the IGM (e.g., Miralda-Escudé 1998). However, following Loeb et al. (2005) we estimated that these two galaxies alone cannot generate a large enough H II region, suggesting either the existence of additional ionizing sources in their vicinity (Dayal et al. 2009, 2011) or the contribution of active galactic nuclei (AGN) activity.

We identified such potential, fainter re-ionizers through a follow-up *Hubble Space Telescope* (*HST*) program (Castellano et al. 2016, hereafter C16a). The dropout selection yielded a total of six additional highly reliable $z > 6.5$ candidates at S/N (Y105) > 10, corresponding to a number density ≳3–4 times higher than expected on the basis of the $z = 7$ ultraviolet (UV) luminosity function (Bouwens et al. 2015; Finkelstein et al. 2015). A stacking of the available *HST* and VLT images confirmed that these are robust $z \sim 7$ sources. A comparison between observations and cosmological simulations (Hutter et al. 2014, 2015) showed that this BDF overdensity has all expected properties of an early reionized region embedded in a half neutral IGM.

In this Letter we present deep spectroscopic follow-up of these additional LBGs aimed at estimating their Lyα fraction and redshift. If the BDF hosted a reionized *bubble* we would expect to measure a Lyα fraction higher than in average $z \sim 7$ lines of sight and more consistent with the one measured at $z \sim 6$. The BDF is the first $z \sim 7$ field where a test of this kind

can be performed. The observations are described in Section 2, while results and the estimate of the Lyα fraction are presented in Sections 3 and 4, respectively. Finally, we discuss potential interpretations of our findings and directions for future investigations in Section 5. Throughout the Letter, observed and rest-frame magnitudes are in the AB system, and we adopt the ΛCDM concordance model ($H_0 = 70\,\mathrm{km\,s^{-1}\,Mpc^{-1}}$, $\Omega_M = 0.3$, and $\Omega_\Lambda = 0.7$).

2. Observations

We observed the *HST*-selected candidates with FORS2 on the European Southern Observatory (ESO) VLT, adopting the same setup used in our previous works that proved to be highly successful for confirming $z \sim 7$ galaxies. We used the 600z+23 (OG590) grism (resolution $R = 1390$), with slits $1''$ wide and a length in the range $6''$–$12''$. This setup maximizes the number of observed targets, while enabling a robust sky subtraction and the maximum efficiency in the wavelength range 8000–10100 Å.

Our primary targets in the BDF overdensity around the two Lyα emitters are the six S/N(Y105) > 10 LBGs presented in C16a, plus additional eight sources at S/N(Y105) ∼ 5–10. All of these sources have magnitude in the range Y105 ∼ 26–27.3. We also re-observe the two bright emitters from V11. The mask was observed for a total of 29 hr, resulting in 22.5 hr of net integration time after excluding overheads and low-quality frames.

3. Results

3.1. A New Confirmed Emitter

Out of the 16 candidates observed we confirm one new LBG with bright Lyα emission (Figure 1), BDF2195 at mag Y105 ∼ 26. This object was also detected in the HAWKI Y-band catalog presented in C10b but not included in the high-redshift sample due to photometric uncertainties. We detect a clearly asymmetric Lyα line at $\lambda = 9737$ Å ($z = 7.008$, Figure 2), with FWHM = 240 km s^{-1} (Gaussian fit, corrected for instrumental broadening), and flux $= 1.85 \pm 0.46 \times 10^{-17}$ erg s^{-1} cm^{-2}, corresponding to an EW = 50 Å. IGM absorption affects 22% of this bandpass; accounting for this, and removing line contribution, the corrected Y105 continuum magnitude is 26.2.

Intriguingly, BDF2195 has exactly the same Lyα redshift as BDF521, and the two have a projected physical separation of only 91.3 kpc (Figure 1). No additional lines are clearly found from spectra of the other observed candidates. To determine Lyα detection limits for these other objects, we adapted the simulations presented in F10, V11, P11, P14, and Vanzella et al. (2014) to the new observations (Section 4.1). The typical flux limit is 1.5×10^{-18} erg s^{-1}cm^{-2} in the range 8100–10000 Å, though it varies depending on the exact wavelength, due to the presence of bright sky emission in this spectral range. The corresponding rest-frame equivalent width (EW) limit varies between 10 and 30 Å across the redshift range $z \simeq 6$–7.2. Details of the observed sample are reported in Table 1.

3.2. Limits on NVλ1240 Emission

The wavelength range observed by FORS2 covers the region of NV emission, where however no apparent emission signal is found in any of the three Lyα emitters within 500 km s^{-1} from the expected position of the line (e.g., Mainali et al. 2018), resulting in limits on the ratio Lyα/NV $\gtrsim$ 8–10. We then built a weighted average spectrum of the three emitters (see Figure 2) using all of the data of the present program and of our previous observations to compute limits on the NV emission, under the assumption that the shift between Lyα and NV emission is similar in the three sources. The stacked source has Lyα flux of 16.7×10^{-18} erg s^{-1} cm^{-2} and a NV $< 3.36 \times 10^{-19}$ erg s^{-1} cm^{-2}, corresponding to Lyα/NV > 17. This limit is much higher than the ratios measured in some $z \gtrsim 7$ galaxies and considered indicative of AGN emission, ranging from Lyα/NV ∼ 1–2 (Tilvi et al. 2016; Hu et al. 2017; Sobral et al. 2017) to ≃6–9 (Laporte et al. 2017; Mainali et al. 2018). Our limit is also higher than the average Lyα/NV ∼ 12 found in LBG-selected narrow-line AGNs at $z \sim 2$–3 by Hainline et al. (2011). However, the latter work also find that the Lyα/NV distribution covers a wide range of values and Lyα/NV $\gtrsim$ 20 are found (see also McCarthy 1993; Humphrey et al. 2008). Finally, NV emission might also lack due to a very low metallicity (though BDF3299 is already fairly enriched, as shown by Carniani et al. 2017). It is thus not possible to rule out that our emitters also host AGN activity.

4. The Lyα Visibility in the BDF Region

4.1. Simulations of the Lyα Population at High-redshift

Under the scenario where the BDF region is highly ionized compared to the average $z = 7$ universe, our expectation was to detect Lyα also in several faint galaxies. Instead, we only confirmed one new bright source. To assess the significance of this result we run Monte Carlo simulations to determine the expected number of objects we should have detected if the BDF region was similar in terms of Lyα visibility to the average $z = 7$ universe or to the average $z = 6$ one (i.e., with a greater Lyα visibility).

We consider the 17 sources presented in Table 1, namely the 16 targets discussed in Section 2 plus another bright object (BDF2883 at $Y = 25.97$) that was observed in the same region with the old FORS2 mask (P11 and V11). First, for each object without a confirmed redshift we extract randomly a redshift according to two cases: (a) we assume that the redshift distributions of the candidates follow those derived from the LBG color selection from C16a. These distributions ($P(z, Y)$ in Table 2) are derived from simulations for three Δmag = 0.5 bins at $Y = 26$–27.5, and peak at $z \sim 6.9$ with magnitude-dependent tails covering the range $z \sim 6.0$–7.8; (b) we assume a *flat* redshift distribution in the small redshift range [6.95:7.15] approximately corresponding to a size of 10 Mpc, thus assuming all sources to be part of a unique, localized structure.

When a redshift is assigned, we calculate the rest-frame $M_{\rm UV}$ (at $\lambda = 1500$ Å) of the galaxy on the basis of the observed magnitude assuming a flat spectrum, and we determine the limiting flux at 3σ from the expected position of the Lyα line. We then calculate the limiting Lyα line EW (EW$_{\rm lim}$) on the basis of the limiting flux and the observed magnitude. For all objects with a Lyα detection we fix the redshift at the spectroscopic value and determine $M_{\rm UV}$ and EW$_{\rm lim}$ as above. The observed continuum flux is computed from the observed Y105 magnitude for all sources with no line detection. In the

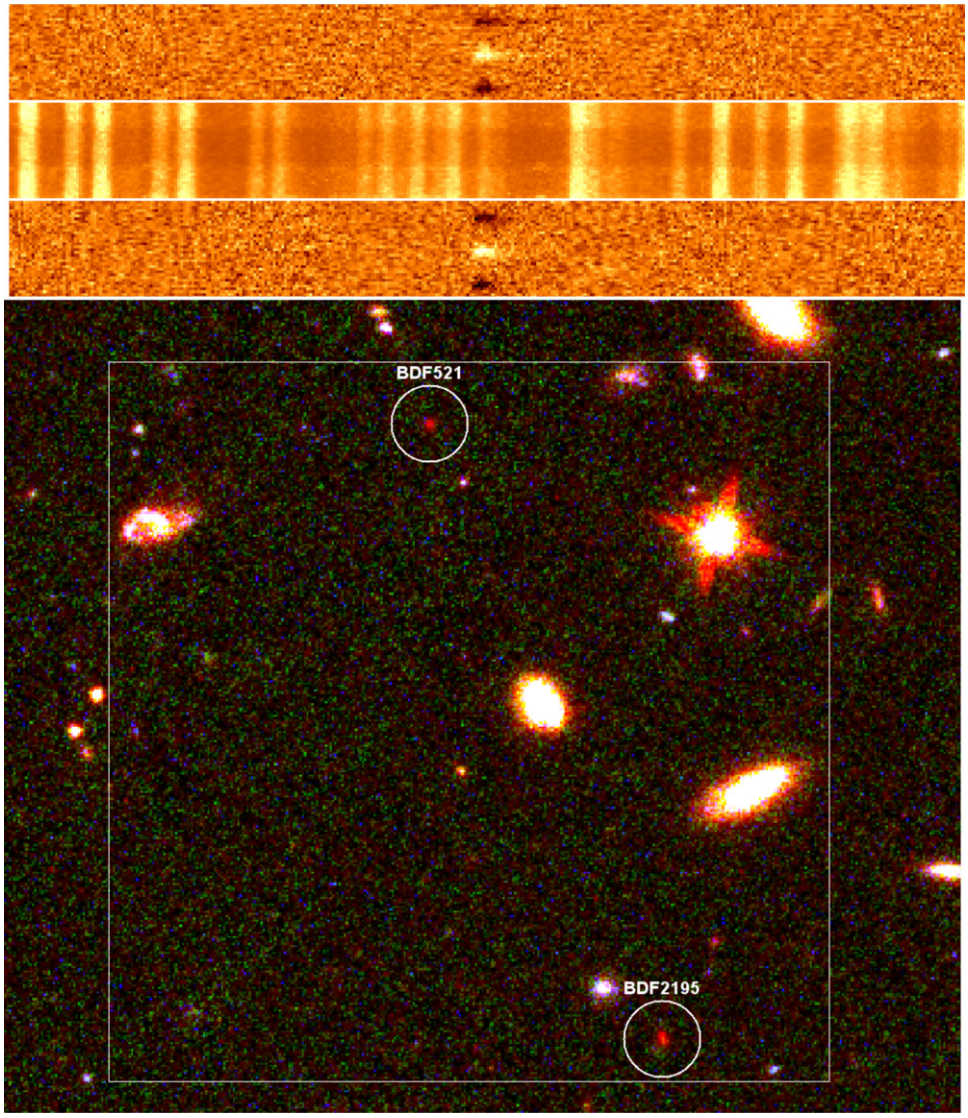

Figure 1. Top: the FORS2 S/N spectra of BDF521 (top) and BDF2195 (bottom) together with the reference rms spectrum (middle). Bottom: the two objects on a *HST* three-color image of the BDF (blue, green, and red channels are V606, I814, and Y105 respectively), the box side is of 100 kpc (physical) at $z = 7.008$.

case of BDF521 and BDF2195 we adopt as reference the J125 magnitude (Cai et al. 2015), which samples the UV at 1500 Å and is not affected by IGM and Lyα emission, while for BDF3299 we correct the observed Y105 magnitude by subtracting line emission and accounting for the portion of filter (27%) sampling IGM. We extract an intrinsic Lyα EW (EW_{intr}) for our object: this is randomly drawn from the observed EW distributions that are derived separately for faint and bright galaxies ($M_{UV} < -20.25$) from more than 160 $z \sim 6$–7 LBGs in the CANDELS fields (Castellano et al. 2017; De Barros et al. 2017, and Pentericci et al. 2018). If $EW_{intr} > EW_{lim}$, then the galaxy is counted as a detection, otherwise it is counted as a nondetection. If the extracted redshift is beyond the FORS2 range ($z \lesssim 7.3$), it is automatically counted as a nondetection. The procedure is repeated 10^5 times for all 17 input objects. As additional input parameter, we can allow a fraction of the objects to be undetected because they are lower redshift interlopers.

We obtain (1) the fraction and total number of expected detections at bright and faint magnitudes; (2) the probability of having a total of 0, 1, 2 etc. detections in each sample, and (3) the EW distribution of the detected objects.

4.2. Prevalence of Bright Lyα Emitters

We find that the number of bright detected objects (3) points to a very high line visibility in this region. In fact, it is higher than expected at $z \sim 7$ and even higher than the $z \sim 6$ statistics, though more consistent with the latter scenario of a "clean" $z \sim 6$-like visibility: the probability of finding three bright emitters given the known $z \sim 7$ Lyα visibility is less than 1%. However, the Lyα fraction among faint galaxies is strikingly at odds with the expectations for the "reionized" case. We expect ~four detections in the faint sample for a $z \sim 6$ EW distribution, and the probability of finding none is 0.2%–0.4%. No appreciable difference is found among the "flat" and "$P(z, Y)$" cases. The results are summarized in Table 2.

Adopting a 5σ threshold, the number of expected detections decreases by 25%–35% for bright sources and 40%–100% for faint ones, depending on the redshift distributions, but remains inconsistent with the observations.

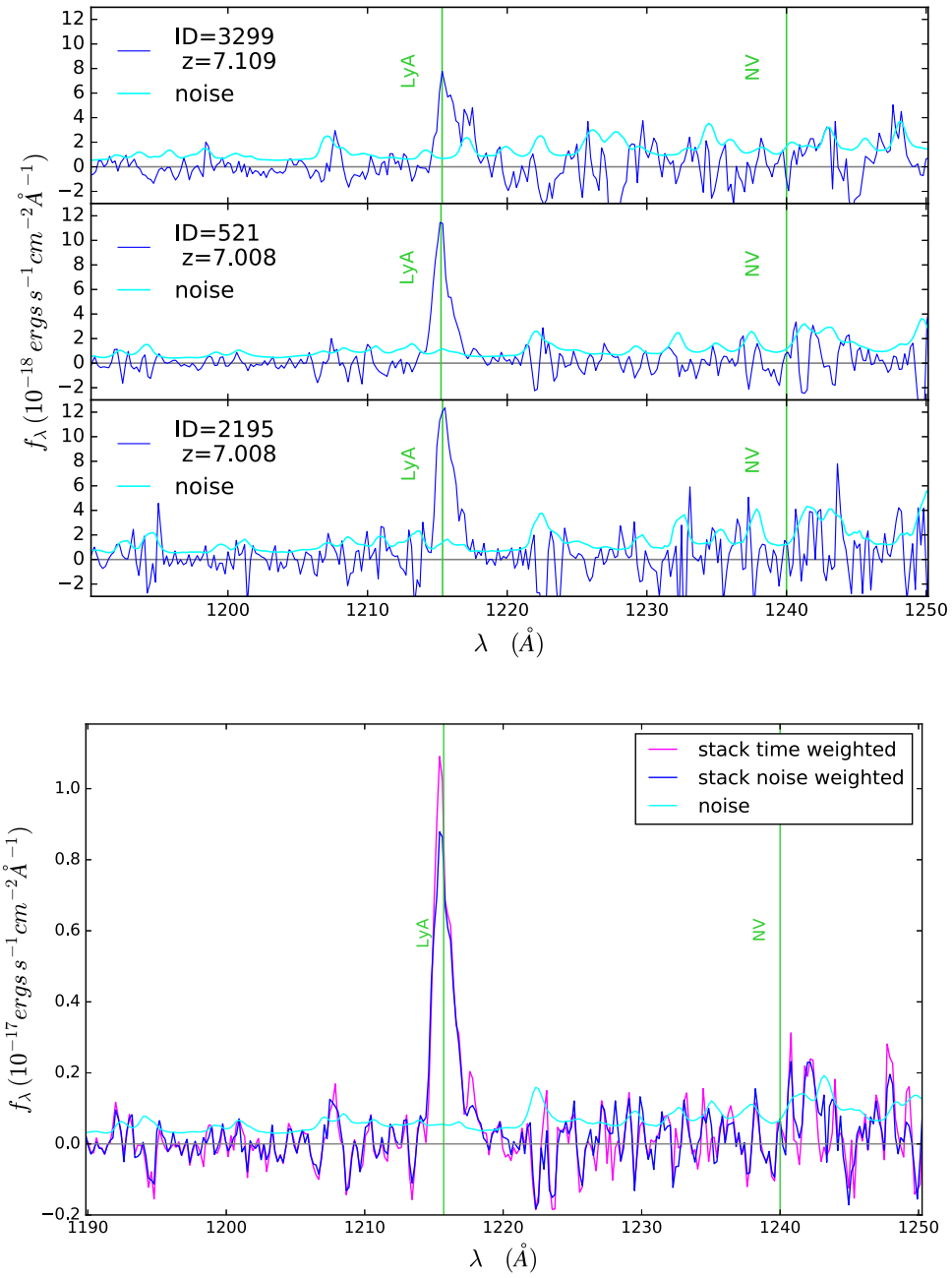

Figure 2. Top: the three LAE in the BDF field: BDF521 and BDF3299 from Vanzella+11 (combining old and new FORS2 data), and the new one, BDF2195. Bottom: the stacked spectrum of the three emitters obtained by scaling them with the total integration time applying a minmax clipping (magenta line), or weighting with the noise spectra (blue line, the resulting sky noise is shown in cyan).

We have so far assumed that all our sources are genuine high-redshift galaxies. Only under the extreme assumption of a $\gtrsim$50%–70% fraction of interlopers at faint end (at 5σ and 3σ thresholds for line identification, respectively), the null Lyα detection rate among faint galaxies can be reconciled with a $z\sim6$ EW distribution at both bright and faint fluxes. We consider this a very unlikely possibility given the conservative selection criteria adopted and the fact that in none of the unconfirmed galaxies do we detect other features that could point to a low-redshift nature.

5. Discussion and Conclusions

The high detection rate of Lyα emission in the BDF bright sources supports the scenario from C16a, namely the BDF hosts a reionized bubble where Lyα visibility is enhanced. However, the lack of Lyα detections in faint galaxies is apparently at odds with such a picture.

Our observations could imply that contrary to the reference scenario outlined in C16a, the faint galaxies are actually outside the bubbles, while the bubbles are created by the bright galaxies alone, or thanks to the contribution of objects beyond the current detection limit (as the $z\sim6$ clustered ultra-faint dwarfs observed by Vanzella et al. 2017a, 2017b). The faint galaxies might be part of a superstructure that includes the reionized regions, but their Lyα might be undetected because they lie outside the patches with low neutral fraction. Unfortunately, the available *HST* imaging observations do not cover the full BDF region ($\sim$2.4 $\times$ 2.4 Mpc at $z\sim7$) but

Table 1
FORS2 $z \sim 7$ Targets: Optical and Spectroscopic Properties

ID	R.A.	Decl.	Y_{105}	Redshift	Lyα EW[a] (Å)
2883	337.028076	−35.160122	25.97 ± 0.08	⋯	<13
2195	336.942352	−35.123257	26.02 ± 0.04	7.008 ± 0.002	50 ± 12
401	337.051239	−35.172020	26.43 ± 0.08	⋯	<11
3299	337.051147	−35.166512	26.52 ± 0.08	7.109 ± 0.002	50 ± 6[b]
521	336.944397	−35.118809	26.53 ± 0.07	7.008 ± 0.002	64 ± 6[b]
2009	336.933716	−35.124950	26.89 ± 0.14	⋯	<17
994	336.957092	−35.136780	27.11 ± 0.19	⋯	<19
1147	337.027130	−35.163212	27.26 ± 0.11	⋯	<22
2660	336.940186	−35.116970	27.27 ± 0.10	⋯	<22
2980	337.024994	−35.142494	27.30 ± 0.12	⋯	<22
647	337.034332	−35.168716	27.31 ± 0.15	⋯	<23
1310	336.953339	−35.133030	27.32 ± 0.16	⋯	<23
2391	337.051361	−35.149185	27.33 ± 0.17	⋯	<23
187	336.953186	−35.147457	27.33 ± 0.10	⋯	<23
1899	336.958618	−35.126297	27.35 ± 0.15	⋯	<23
1807	337.057861	−35.155842	27.36 ± 0.09	⋯	<24
2192	337.018158	−35.151600	27.40 ± 0.10	⋯	<25

Notes.
[a] Average 3σ upper limits are computed at $7.008 \leqslant z \leqslant 7.109$.
[b] From V11.

Table 2
Top: the Observed Number of Bright and Faint Candidates, Assuming Sources to be at $z = 7$ ($M_{\rm UV} < -20.25$ Corresponding to $Y_{105} < 26.7$)

Sample	Total	Bright	Faint
Observed	17	5	12
Detected in Lyα	3	3	0

PDF(z)	Lyα Visibility	Probability P(tot = 3)	P(bright = 3)	P(faint = 0)	Expected Number $\langle N_{\rm tot}\rangle$	$\langle N_{\rm bright}\rangle$	$\langle N_{\rm faint}\rangle$
Flat	$z = 7$	0.21	0.009	0.17	2.1	0.7	1.4
$P(z, Y)$	$z = 7$	0.18	0.009	0.22	1.9	0.7	1.2
Flat	$z = 6$	0.08	0.035	0.002	5.5	1.2	4.3
$P(z, Y)$	$z = 6$	0.11	0.036	0.004	5.0	1.2	3.8

Note. Bottom: probability of observed 3σ Lyα detections, and expected number of detected lines for the total, bright, and faint subsamples, as computed from Monte Carlo simulations.

only two $\sim 0.7 \times 0.7$ Mpc areas centered on the emitters, thus preventing detailed constraints on the extent and geometry of the overdensity.

To ascertain whether or not the BDF emitters are capable of re-ionizing their surroundings, we performed spectral energy distribution (SED)-fitting on the available photometry (see C16a for details) and estimated the star formation rate (SFR) and ionizing flux of the BDF emitters with our χ^2 minimization code *zphot.exe* (Fontana et al. 2000). The SFR and the age of the galaxies are then used to measure the size ($R_{\rm bubble}$) of the resulting ionized bubbles assuming a hydrogen clumping factor $C = 2$ and an average neutral hydrogen fraction $\chi_{\rm H\,I} = 0.5$ surrounding the sources at the onset of star formation (see, e.g., Shapiro & Giroux 1987; Madau et al. 1999). We used both BC03 (Bruzual & Charlot 2003) and BPASSV2.0 (Eldridge & Stanway 2009; Stanway et al. 2016) templates with constant SFR, aged from 1 Myr to the age of the universe at the given redshift, $E(B - V)$ in the range 0.0–1.0 (assuming the Calzetti et al. 2000 extinction curve) and metallicity from $0.02Z_{\odot}$ to solar. In Figure 3 we show the $R_{\rm bubble}$ of the ionized regions created by BPASS SED models within 68% c.l. from the best fit for the three emitters, as a function of the age of the stellar population and for different values of the $f_{\rm esc}$. We also show the $R_{\rm bubble}$ ranges for the case where we summed together the ionizing fluxes of the two sources BDF521 and BDF2195 that form a close pair at only ∼90 kpc projected separation. The size $R_{\rm bubble}$ must be compared to the dimension $R_{\rm min} = 1.1$ Mpc (estimated as in Loeb et al. 2005), enabling Lyα to be redshifted enough to reach the observers.

On the one hand, BDF521 and BDF2195 would require a high $f_{\rm esc} \gtrsim 20\%$–60% to create a large enough bubble, while BDF3299 is unable to create its own bubble even assuming 100% escape fraction. On the other hand, when summing the two contributions the BDF521–BDF2195 pair can create a large enough bubble with $f_{\rm esc} \gtrsim 10\%$–15% (BC03 and BPASSV2, respectively) and constant star formation for $\gtrsim$400 Myr. We do not find solutions that allow age <20 Myr, which is also consistent with supernovae requiring 3.5–28 Myr to build channels that can allow LyC photons to escape (Ferrara & Loeb 2013). We find that results obtained with BPASSV2 library point to slightly higher re-ionizing capabilities compared to BC03 ones, as slightly smaller fitted SFRs partially

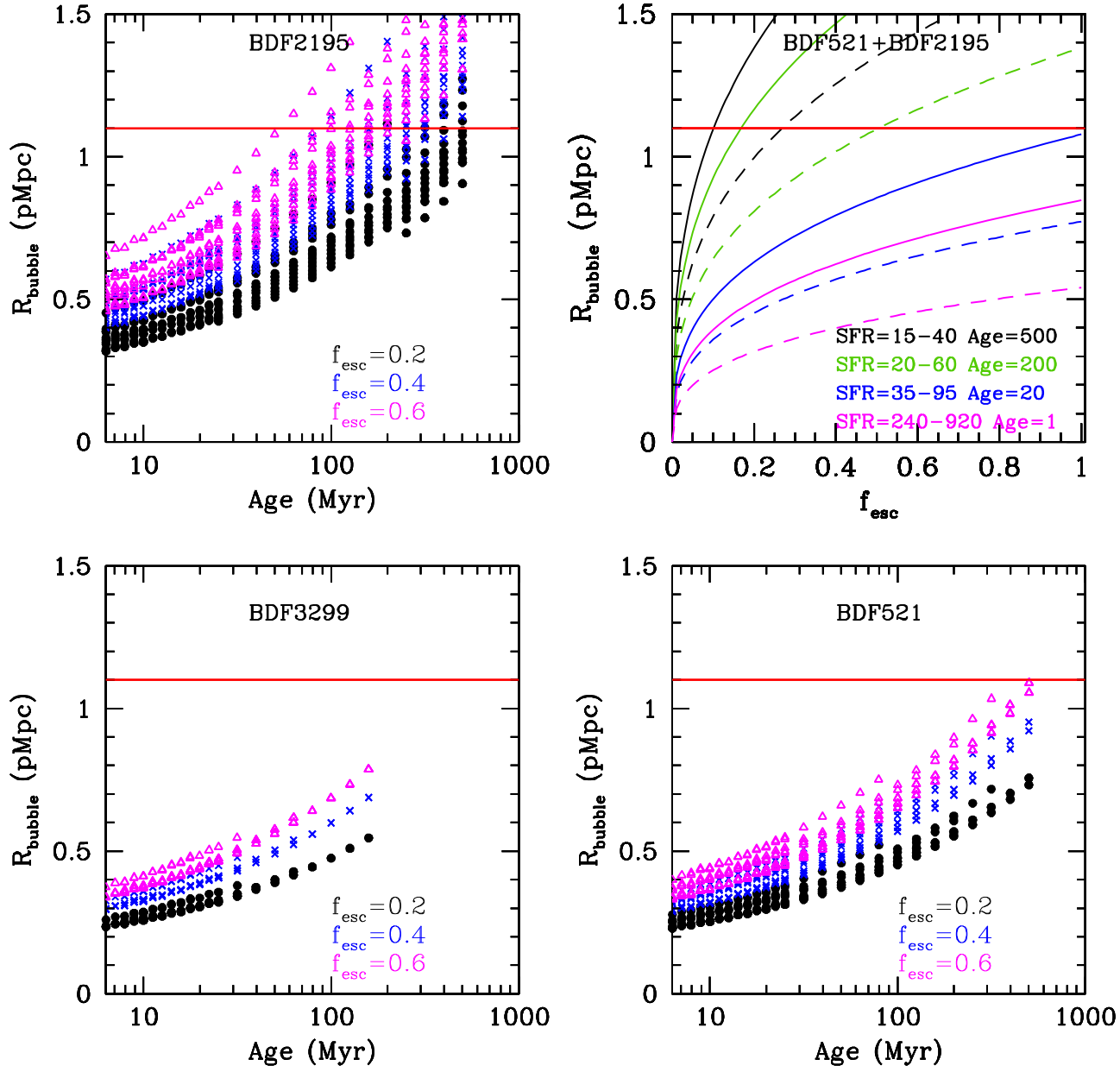

Figure 3. Size ($R_{\rm bubble}$) of the ionized bubbles created by the three emitters, as a function of the age of the stellar population (bottom panels and top-left panel) for BPASSV2 SED models within 68% c.l. from the best fit. The cases for escape fraction $f_{\rm esc} = 0.2$, 0.4, 0.6 are shown as black circles, blue crosses, and magenta triangles, respectively. Solutions having the same age and $f_{\rm esc}$ differ in terms of either best-fit metallicity or $E(B-V)$, or both. The top-right panel show minimum (dashed lines) and maximum (continuous lines) $R_{\rm bubble}$ as a function of $f_{\rm esc}$ adding contribution from BDF521 and BDF2195, for stellar populations of age 500 (black), 200 (green), 20 (blue), and 1 Myr (magenta). The horizontal red line in all plots mark the minimum H II size $R_{\rm min} = 1.1$ Mpc, enabling Lyα to escape.

compensate for the higher ionizing photons production rate of the BPASS models. The aforementioned $R_{\rm min}$ assumes that the Lyα escapes from the galaxies at the systemic redshift. However, line visibility from smaller H II regions is possible in the presence of strong outflows: a 220 km s^{-1} shift, which is the median value for galaxies in massive halos from Mason et al. (2018), results in $R_{\rm min} \sim 0.85$ Mpc; this can be reached in a few 100 Myr by the BDF521–BDF2195 pair with $f_{\rm esc} \lesssim 10\%$, but still out of reach for BDF3299 without extreme $f_{\rm esc}$.

The case described above considers star formation as the only source of ionizing photons. However, we cannot exclude the fact that the BDF emitters host AGN that could provide a substantial contribution to the ionizing budget, or that the bubbles have been created by past AGN activity. In such a case, bright emitters including BDF3299 could be solely responsible for the creation of reionized regions, assuming lower $f_{\rm esc}$ and/or ages for their stellar populations.

As an alternative to scenarios where the ionizing flux is generated by bright galaxies alone, some mechanisms must be in place to prevent Lyα from faint galaxies to reach the observers. A possible explanation can be found in an accelerated evolution of overdensity members compared to the normal field population. The bright emitters are young, relatively dust-free sources (consistent with the Atacama Large Millimeter/submillimeter Array (ALMA) results from Maiolino et al. 2015) experiencing a bursty episode of star formation. Intense bursts of star formation favoring the escape of Lyα photons are stimulated by an enhanced rate of mergers and interactions within the overdensity.

In this picture, all faint LBGs are actually more evolved objects, thus with intrinsically fainter line emission, that have already experienced such bursty star formation episodes in the past. The recombination of neutral hydrogen in the regions close to overdensity members can provide an additional mechanism for explaining lack of line emission from faint galaxies, as it is only in bright galaxies with large circular velocities that Lyα photons acquire a frequency shift enabling their escape from the circumgalactic medium.

Indeed, as discussed by Mason et al. (2018), Lyα emission from UV bright galaxies residing in reionized overdensities can be further boosted by their higher velocity offsets that reduce the damping wing absorption by cosmic neutral hydrogen. This effect, possibly along with enhanced Lyα photon production, has been proposed as a physical explanation for the increased Lyα visibility in very bright ($M_{\rm UV} < -22$) $z > 7$ galaxies found by Stark et al. (2017). While the three BDF emitters at $M_{\rm UV} \gtrsim -21$ are not as bright, the combination of a large enough H II region around them, and of frequency shifts induced by their circular velocities, likely plays a role in enhancing their Lyα visibility with respect to $z \sim 6$ LBGs.

Luckily, a thorough examination of the aforementioned scenarios will soon be made possible by observations with the *James Webb Space Telescope* (*JWST*). It will be possible to (1) confirm a very low neutral fraction in the region surrounding the bright emitters by looking for blue wings in high-resolution Lyα spectra (e.g., Hu et al. 2016); (2) clarify the nature of bright emitters through a more accurate measurement of SFR, extinction, and age (Hα luminosity, Hα/Hβ, and Hα/UV ratios), and probing signatures of a high escape fraction (EW of Balmer lines or the O_{32} ratio, e.g., de Barros et al. 2016; Castellano et al. 2017; Chisholm et al. 2018), AGN emission, and hard ionizing stellar spectra (e.g., Mainali et al. 2017; Senchyna et al. 2017); (3) assess whether faint candidates are members of a localized overdensity at $z \simeq 7.0$–7.1 as the bright ones, or just outside such a region, or low-z interlopers in the sample by measuring their redshift from optical emission lines; and (4) measure velocity shifts between Lyα and UV/optical lines that trace the systemic redshift of bright emitters.

A systematic analysis of this kind carried out with *JWST* on $z \gtrsim 7$ lines of sight with different levels of Lyα visibility will eventually shed light on the processes responsible for the creation of the first reionized regions.

Based on observations collected at the European Organisation for Astronomical Research in the Southern Hemisphere under ESO programme 099.A-0671(A). P.D. acknowledges support from the European Research Council's starting grant ERC StG-717001 and from the European Commission's and University of Groningen's CO-FUND Rosalind Franklin program.

ORCID iDs

M. Castellano https://orcid.org/0000-0001-9875-8263
L. Pentericci https://orcid.org/0000-0001-8940-6768
E. Vanzella https://orcid.org/0000-0002-5057-135X
A. Fontana https://orcid.org/0000-0003-3820-2823
P. Dayal https://orcid.org/0000-0001-8460-1564
A. Ferrara https://orcid.org/0000-0002-9400-7312
A. Hutter https://orcid.org/0000-0003-3760-461X
S. Carniani https://orcid.org/0000-0002-6719-380X
M. Dickinson https://orcid.org/0000-0001-5414-5131
E. Giallongo https://orcid.org/0000-0003-0734-1273
M. Giavalisco https://orcid.org/0000-0002-7831-8751
A. Grazian https://orcid.org/0000-0002-5688-0663
P. Santini https://orcid.org/0000-0002-9334-8705

References

Bouwens, R. J., Illingworth, G. D., Oesch, P. A., et al. 2015, ApJ, 803, 34
Bruzual, G., & Charlot, S. 2003, MNRAS, 344, 1000
Cai, Z., Fan, X., Jiang, L., et al. 2015, ApJL, 799, L19
Calzetti, D., Armus, L., Bohlin, R. C., et al. 2000, ApJ, 533, 682
Carniani, S., Maiolino, R., Pallottini, A., et al. 2017, A&A, 605, A42
Caruana, J., Bunker, A. J., Wilkins, S. M., et al. 2012, MNRAS, 427, 3055
Castellano, M., Dayal, P., Pentericci, L., et al. 2016, ApJL, 818, L3
Castellano, M., Fontana, A., Paris, D., et al. 2010, A&A, 524, A28
Castellano, M., Pentericci, L., Fontana, A., et al. 2017, ApJ, 839, 73
Chisholm, J., Gazagnes, S., Schaerer, D., et al. 2018, arXiv:1803.03655
Dayal, P., Ferrara, A., Saro, A., et al. 2009, MNRAS, 400, 2000
Dayal, P., Maselli, A., & Ferrara, A. 2011, MNRAS, 410, 830
De Barros, S., Pentericci, L., Vanzella, E., et al. 2017, A&A, 608, A123
de Barros, S., Vanzella, E., Amorín, R., et al. 2016, A&A, 585, A51
Eldridge, J. J., & Stanway, E. R. 2009, MNRAS, 400, 1019
Ferrara, A., & Loeb, A. 2013, MNRAS, 431, 2826
Finkelstein, S. L., Ryan, R. E., Jr., Papovich, C., et al. 2015, ApJ, 810, 71
Fontana, A., D'Odorico, S., Poli, F., et al. 2000, AJ, 120, 2206
Fontana, A., Vanzella, E., Pentericci, L., et al. 2010, ApJL, 725, L205
Hainline, K. N., Shapley, A. E., Greene, J. E., & Steidel, C. C. 2011, ApJ, 733, 31
Hu, E. M., Cowie, L. L., Songaila, A., et al. 2016, ApJL, 825, L7
Hu, W., Wang, J., Zheng, Z.-Y., et al. 2017, ApJL, 845, L16
Humphrey, A., Villar-Martín, M., Vernet, J., et al. 2008, MNRAS, 383, 11
Hutter, A., Dayal, P., & Müller, V. 2015, MNRAS, 450, 4025
Hutter, A., Dayal, P., Partl, A. M., & Müller, V. 2014, MNRAS, 441, 2861
Laporte, N., Nakajima, K., Ellis, R. S., et al. 2017, ApJ, 851, 40
Lehnert, M. D., & Bremer, M. 2003, ApJ, 593, 630
Loeb, A., Barkana, R., & Hernquist, L. 2005, ApJ, 620, 553
Madau, P., Haardt, F., & Rees, M. J. 1999, ApJ, 514, 648
Mainali, R., Kollmeier, J. A., Stark, D. P., et al. 2017, ApJL, 836, L14
Mainali, R., Zitrin, A., Stark, D. P., et al. 2018, MNRAS, 479, 1180
Maiolino, R., Carniani, S., Fontana, A., et al. 2015, MNRAS, 452, 54
Mason, C. A., Treu, T., de Barros, S., et al. 2018, ApJL, 857, L11
McCarthy, P. J. 1993, ARA&A, 31, 639
Miralda-Escudé, J. 1998, ApJ, 501, 15
Pentericci, L., Fontana, A., Vanzella, E., et al. 2011, ApJ, 743, 132
Pentericci, L., McLure, R. J., Garilli, B., et al. 2018, A&A, submitted
Pentericci, L., Vanzella, E., Fontana, A., et al. 2014, ApJ, 793, 113
Schenker, M. A., Stark, D. P., Ellis, R. S., et al. 2012, ApJ, 744, 179
Senchyna, P., Stark, D. P., Vidal-García, A., et al. 2017, MNRAS, 472, 2608
Shapiro, P. R., & Giroux, M. L. 1987, ApJL, 321, L107
Sobral, D., Matthee, J., Brammer, G., et al. 2017, arXiv:1710.08422
Stanway, E. R., Eldridge, J. J., & Becker, G. D. 2016, MNRAS, 456, 485
Stark, D. P., Ellis, R. S., Charlot, S., et al. 2017, MNRAS, 464, 469
Stark, D. P., Ellis, R. S., Chiu, K., Ouchi, M., & Bunker, A. 2010, MNRAS, 408, 1628
Tilvi, V., Pirzkal, N., Malhotra, S., et al. 2016, ApJL, 827, L14
Vanzella, E., Calura, F., Meneghetti, M., et al. 2017a, MNRAS, 467, 4304
Vanzella, E., Castellano, M., Meneghetti, M., et al. 2017b, ApJ, 842, 47
Vanzella, E., Fontana, A., Zitrin, A., et al. 2014, ApJL, 783, L12
Vanzella, E., Pentericci, L., Fontana, A., et al. 2011, ApJL, 730, L35